Optical Materials 33 (2011) 1530–1534

Contents lists available at ScienceDirect

Optical Materials

journal homepage: www.elsevier.com/locate/optmat

Application of photoconductivity measurements to photodynamic processes investigation in $LiYF_4:Ce^{3+}$ and $LiLuF_4:Ce^{3+}$ crystals

L. Nurtdinova [a,*], V. Semashko [a], Y. Guyot [b], S. Korableva [a], M.-F. Joubert [b], A. Nizamutdinov [a]

[a] Kazan (Volga Region) Federal University, 18 Kremlevskaya St., 420008 Kazan, Russia
[b] Université de Lyon, Université Lyon 1, CNRS, UMR5620, LPCML, F-69622 Villeurbanne Cedex, France

ARTICLE INFO

Article history:
Received 15 October 2010
Received in revised form 11 March 2011
Accepted 11 March 2011
Available online 6 April 2011

Keywords:
Photodynamic processes
Photoconductivity
Excited-state photoionization
Rare-earth ions
Fluoride crystals
UV active media

ABSTRACT

Photoconductivity measurements are applied to the studies of photodynamic processes in $LiYF_4:Ce^{3+}$ and $LiLuF_4:Ce^{3+}$ crystals undergoing ultraviolet irradiation. Photoconductivity spectra were registered by means of microwave technique under irradiation at 220–320 nm at the room temperature. Photoconductivity signal appeared at ~300 nm and monotonically increased with the shortening of wavelength. Pumping energy dependencies of photoconductivity within 225–305 nm spectral range were registered and revealed the change of the dependence degree from quadratic at longer wavelengths through linear to saturation-like at shorter ones. Numerical simulation based on four-level model of photodynamic processes was performed. Values and spectral distributions of probabilities of different types of photodynamic processes for 225–295 nm were estimated. Ce^{3+} ions excited-state photoionization cross-section spectra in both investigated materials revealed a band with a peak around 270 nm most probably corresponding to 5d–6s transition of Ce^{3+}. Recombination cross-section in $Ce:LiLuF_4$ appeared to be two orders of magnitude higher than in $Ce:LiYF_4$. A complete energy level diagram of "Ce^{3+} ion–$LiYF_4$ crystal" system has been proposed.

1. Introduction

The advancement of science and industry causes demand for compact, inexpensive and reliable UV lasers preferably with a wide tuning range. However, in the majority of solid-state active media UV radiation induces so-called photodynamic processes (PDP) [1]. Such processes as excited-state absorption followed by ionization of activator ions (excited-state photoionization or ESP), color centers formation and so on are usually considered harmful and lead to the degradation of active media performance.

Photodynamic processes involve not only intracenter transitions of active ions but transitions to the energy levels of crystal lattice as well [2]. Therefore, in order to create an adequate model of these processes it is essential to know how energy states of the both subsystems are situated relative to each other. It is rather difficult to provide such a complete energy level diagram solely by means of traditional spectroscopy because of the overlapping of spectra corresponding to the activator ions, color centers and crystal lattice itself, on the one hand, and the certain experimental difficulties arising in the short-wave range of the UV spectral region (VUV), on the other. And this is where photoconductivity measurements could be of use. The fact is that photoconductivity technique allows direct studies of PDP. It is based on registration of the free charge carriers' formation in the conduction and valence bands of the insulating material undergoing UV irradiation [3].

This investigation aims to apply photoconductivity measurements to the investigation of PDP. As a result numerical and spectral characteristics of PDP are determined and applied to construct a complete energy level diagram of the joint "activator ion–crystal lattice" system.

2. Investigated materials

Ce^{3+}-activated $LiYF_4$ (LYF) and $LiLuF_4$ (LLF) crystals are well-known active media for UV lasers since the end of the last century [4,5]. However, under UV radiation both materials are subjected to a strong coloration effect deteriorating their performances, which makes these crystals excellent model objects for the investigation.

Samples used here have been grown and prepared in the Laboratory of crystal growth of Kazan Federal University by means of Bridgman technique in graphite crucibles. As a result pure as well as Ce^{3+}-activated (1 at.% in the melt) LYF and LLF crystals were grown and 2 mm thick disk-shaped samples with two polished surfaces were prepared. Optical axes of the samples were situated in the planes of the polished surfaces.

3. Experimental technique

Microwave technique of photoconductivity registration was adopted from EPR-spectroscopy and is thoroughly described in

* Corresponding author. Tel.: +7 9172603698; fax: +7 8432927499.
E-mail address: ne.goruj@gmail.com (L. Nurtdinova).

0925-3467/$ - see front matter © 2011 Elsevier B.V. All rights reserved.
doi:10.1016/j.optmat.2011.03.028

[6]. Unlike the conventional technique with attachable electrodes [7] generally used in the semiconductor physics this method have the advantages of non-contactness, higher sensibility and allows registration of photoconductivity decays in the tenth of nanoseconds time domain. The sample is placed inside the cavity resonator in the maximum of the electric component of microwave field supplied by Gunn oscillator. Adjusting the coupling between the cavity and the waveguide it is necessary to obtain the minimum of the microwave power reflected from the cavity with the sample inside. When the sample is subjected to UV irradiation, photodynamic processes occur, which leads to the variation of sample's permittivity. Moreover, not only the real part of permittivity is varied, but also it gains an imaginary part, which is proportional to photoinduced electric conductivity according to the following equation:

$$\Delta\varepsilon = \Delta\varepsilon' - i\frac{\sigma_S}{\omega} \quad (1)$$

where ε is the complex permittivity of the material, ε' is its real part, ω is the angular frequency of the microwave electric field, σ_S is the conductivity of the material. Such variation of sample's permittivity causes variations of the quality factor and resonance frequency of the cavity. Therefore, the reflected part of the microwave power increases, and this change is registered.

Reflected power signal contains two components. The first one, so-called "absorption mode", is determined by the variation of the quality factor of the cavity, which, in turn, is proportional to the induced electric conductivity of the sample. As, in fact, the absorption mode signal corresponds to the photoconductivity of the material, hereinafter it will be referred to as photoconductivity signal. The second component is called the "dispersion mode". It is determined by the variation of the resonance frequency of the cavity due to the electron density redistribution as a result of Ce^{3+} absorption, electrons captured by the structural defects of the host, etc.

4. Results and discussion

Using microwave setup [6], built in the "Laboratoire de Physico-Chimie des Matériaux Luminescents" of the Université Claude-Bernard Lyon 1, and pulsed OPO laser (Continuum®, 10 Hz, idler SH 205–340 nm) as a pumping source photoconductivity spectra were registered in the spectral range between 225 and 320 nm. As it can be seen from the Fig. 2b spectrum structure of the dispersion mode signal matches the one of Ce^{3+} ions ground-state absorption in this region. For the undoped LLF and LYF samples no structure in similar spectra was observed.

Photoconductivity signal appears at wavelengths shorter than 300 nm and monotonically increases with the following shortening of excitation radiation wavelength (Fig. 1a). Similar but considerably less (one order of magnitude) intense monotonic increase was demonstrated by the undoped LLF and LYF samples. This is probably caused by the impurity traces in the nominally pure materials. However, due to the previously mentioned overlapping of the ground-state and excited-state absorption spectra of Ce^{3+} ions with the absorption spectra of color centers and the crystal lattice itself different PDP may camouflage one another. In order to separate them and to determine their numerical and spectral characteristics photoconductivity signal for the different values of pumping energy per pulse have been registered in 225–295 nm spectral region. As it can be seen from the Fig. 2a the character of the dependence changes from square at the longer wavelengths through linear and to saturation-like at the shorter ones.

To adequately interpret these data numerical simulation was carried out. It is based on the four-level model of photodynamic processes, which has been developed and successfully applied before [1]. According to this model (Fig. 2b) stepwise absorption of

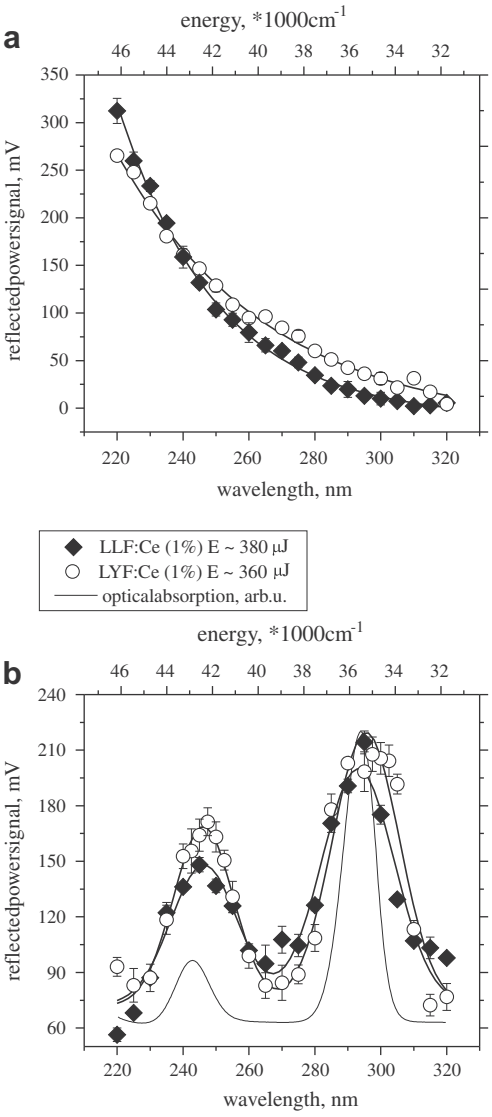

Fig. 1. Photoconductivity spectra of LYF:Ce^{3+} and LLF:Ce^{3+} crystals in absorption (a) and dispersion (b) modes registered at the room temperature.

two photons of pumping radiation by activator ion may be followed by its ionization. It leads to the formation of the free electrons in the conduction band of the host which may contribute to the conductivity of the material. These electrons may stay near the position of Ce ion and recombine with the hole, or detach from Ce and migrate through the crystal to be captured by the structural defect of the lattice creating a color center. The color centers will be eventually bleached either optically (via absorption of pumping radiation or Ce luminescence), or thermally. However, since no change in Ce^{3+} absorption lines intensities is observed after exciting radiation has been applied, it is reasonable to assume that Ce^{4+} ion quickly restores its valence to 3+ due to the capture of the electron from the valence band, thereby, creating a hole near its site. This fact accounts for the hole-type color centers, observed in $LiY_xLu_{1-x}F_4$ ($x = 0, \ldots, 1$) crystals under excitation resonant to 4f–5d transitions of Ce^{3+} [8,9]. Later holes will recombine with the free electrons, and the energy released as a result of such recombination will be transferred to the impurity center contributing to the fluorescence of the latter [10].

On the basis of this model the following system of rate equations was written:

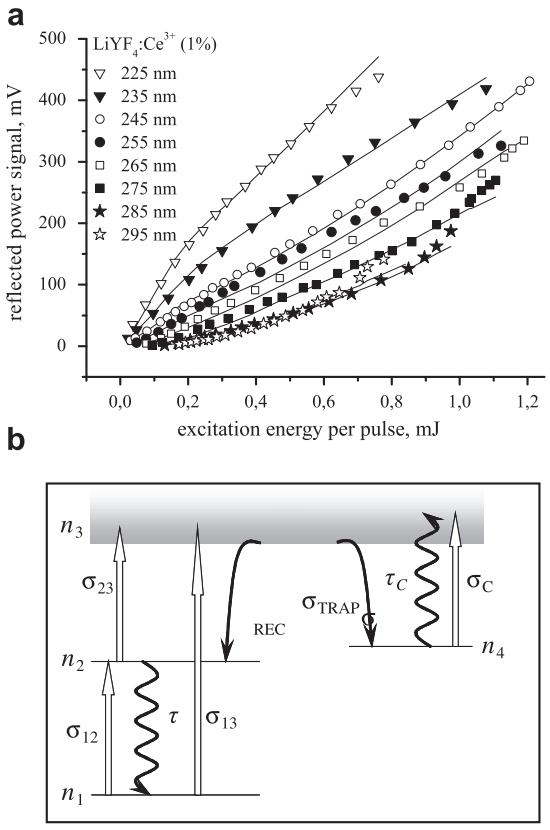

Fig. 2. (a) Reflected power (photoconductivity) signal in absorption mode against pumping radiation energy per pulse for different pumping wavelengths in 225–295 nm region in LYF:Ce^{3+} (1%). T = 300 K. Dots represent experimental data. Solid lines represent fitting results.(b) Four-level model of photodynamic processes, where 1, 2 – energy levels of Ce^{3+} ground and 5d-excited states, 3 – conduction band of the lattice, 4 – energy levels of traps; n_1, n_2, n_3, n_4 – populations of the levels 1,2,3,4; τ – radiative lifetime of Ce^{3+} lowest 5d-excited state, σ_{12} – Ce^{3+} ground-state absorption cross-section, σ_{23} – Ce^{3+} two-photon ionization cross-section, σ_{13} – Ce^{3+} one-photon ionization cross-section, σ_C – color centers ionization cross-section, σ_{rec}, σ_{trap} – free charge carriers recombination and trapping cross-sections, τ_C – average lifetime of color centers at the room temperature.

$$\begin{cases} \frac{dn_1}{dt} = -U(t,\lambda)\cdot\sigma_{12}(\lambda)n_1 + \frac{1}{\tau}n_2 - U(t,\lambda)\sigma_{13}\lambda n_1 \\ \frac{dn_2}{dt} = U(t,\lambda)\cdot\sigma_{12}(\lambda)n_1 - \frac{1}{\tau}\cdot n_2 - U(t,\lambda)\cdot\sigma_{23}(\lambda)\cdot + \sigma_{rec}\cdot\upsilon\cdot(n_3+n_4)\cdot n_3 \\ \frac{dn_3}{dt} = U(t,\lambda)\cdot\sigma_{23}(\lambda)\cdot + U(t,\lambda)\sigma_{13}(\lambda)\cdot n_1 + \frac{1}{\tau_c}\cdot n_4 + U(t,\lambda)\cdot\sigma_c(\lambda)\cdot n_4 \\ \quad -\left[\sigma_{rec}\cdot\upsilon\cdot(n_3+n_4) + \sigma_{trap}\cdot\upsilon\cdot(n_c-n_4)\right]\cdot n_3 \\ \frac{dn_4}{dt} = \sigma_{trap}\cdot\upsilon\cdot(n_c-n_4)\cdot n_3 - \frac{1}{\tau_c}\cdot n_4 - U(t,\lambda)\cdot\sigma_c(\lambda)\cdot n_4 \\ N = n_1+n_2+n_3+n_4 \end{cases} \quad (2)$$

where 1, 2 – energy levels of Ce^{3+} ground and excited states, 3 – conduction band of the lattice, 4 – energy levels of traps; n_1, n_2, n_3, n_4 – populations of levels 1,2,3,4; $U(t, \lambda)$ – exciting radiation pulse at the wavelength λ in units of photon flux density; τ – radiative lifetime of Ce^{3+} lowest 5d-excited state; $\sigma_{12}(\lambda)$ – Ce^{3+} ground-state absorption cross-section; $\sigma_{23}(\lambda)$ – Ce^{3+} two-photon ionization cross-section; $\sigma_{13}(\lambda)$ – Ce^{3+} one-photon ionization cross-section; $\sigma_C(\lambda)$ – color centers ionization cross-section; σ_{rec}, σ_{trap} – free charge carriers recombination and trapping cross-sections; υ – velocity of the free electrons in the conduction band; τ_C – average lifetime of color centers at the room temperature; n_C – concentration of traps; N – concentration of the impurity ions in the media. It should be mentioned that system (2) may be solved for the fixed value of excitation radiation wavelength.

The following processes are taken into account in system (2). Terms of $U(t)\cdot\sigma_{ij}\cdot n_i$ type represent the absorption transitions from level i to level j under the exciting radiation $U(t, \lambda)$ and, therefore, describe ground- and excited-state photoionization of the impurity ions as well as photoionization of color centers (terms with σ_C). Processes of electron–hole recombination at the impurity ions are described by the term $\sigma_{rec}\cdot\upsilon\cdot n_3\cdot(n_3 + n_4)$, where $\sigma_{rec}\cdot\upsilon$ characterizes the volume of the effective (in relation to recombination) cylinder, which is "drawn" by the free electron, moving at a rate υ, per second, whereas n_3 and ($n_3 + n_4$) correspond to the number of the free electrons and number of the holes (able to participate in recombination), respectively. Capture of the free electrons by the defects of the host material is described by the $\sigma_{trap}\cdot\upsilon\cdot n_3\cdot(n_C - n_4)$ term. Similarly to the recombination term it determines the number of the meetings of free electrons (n_3) with unoccupied traps ($n_C - n_4$) resulting in the capture of the former per second. The recombination and trapping terms given above are introduced according to [11]. It is necessary to mention, that in order to simplify calculation procedure this model has been developed under the assumption that the majority of holes are localized at the activator ions.

The solution of system (2) for the given excitation wavelength λ provides time distributions of the 1–4 levels populations ($n_1(t), \ldots, n_4(t)$). At the same time photoconductivity signal (see Fig. 2a) is directly proportional to the number of the free electrons, appearing in the conduction band of the sample under UV irradiation, i.e. the population of level 3 of the model as well. Therefore, the dependences of the experimentally established populations of level 3 versus pumping energy per pulse may be fitted with the calculated ones established as a result of numerical solution of system (2).

The fitting procedure is based on the method of variation of parameters. It provides the values and spectral distributions of σ_{23}, σ_{13}, σ_C, σ_{rec}, σ_{trap} parameters of system (2) for the each value of pumping wavelength used in the experiment. Pumping pulse $U(t, \lambda)$ was represented by the Gaussian function with FWHM 5×10^{-9} s. Values of the parameters σ_{12} and τ were estimated from the spectral-kinetic studies of the investigated materials for the each pumping wavelength [10,12] and were not varied in the course of the fitting. Variation of parameter τ_C within wide limits (10^{-9}–10 s) did not significantly affect the results of the approximation. Therefore, it was chosen to be equal to pulse-repetition interval of pumping radiation $\sim 10^{-1}$ s. As no saturation of color centers absorption, generated in these materials under UV irradiation, has been observed with the increase of pumping flux within large limits [13], number of the defects n_C was chosen an order of magnitude greater than the number of the impurity centers N.

Since system (2) cannot be solved analytically, the direct search algorithm [14] has been applied. According to this algorithm system (2) has to be solved numerically after the each variation of the sought parameters. As a convergence criterion the minimum of the squared difference between experimental and calculated energy dependencies of population n_3 was chosen. It should be mentioned, that cross-sections σ_{23}, σ_{13}, σ_C (unlike σ_{rec} and σ_{trap}) vary depending on the pumping wavelength. Therefore, it is necessary to determine these parameters for the each value of pumping wavelength independently. Thus, all eight sets of experimental data (see Fig. 2a), corresponding to the different pumping wavelengths, have been treated simultaneously in the course of the approximation.

Results of the simulation are presented on Fig. 3. Numerical values and spectral distributions of such PDP characteristics as cross-sections of activator and color centers ionization, recombination and trapping of the free electrons by the structural defects of the lattice were determined. Calculated spectrum of Ce^{3+} ionization cross-section from the excited 5d state (see Fig. 3) revealed a band with a peak near 270 nm for the both investigated materials. This fact accounts for the experimentally observed monotonic behavior of photoconductivity signal, presented on Fig. 2. It can be seen from the figure that maximum of Ce^{3+} ground-state absorption

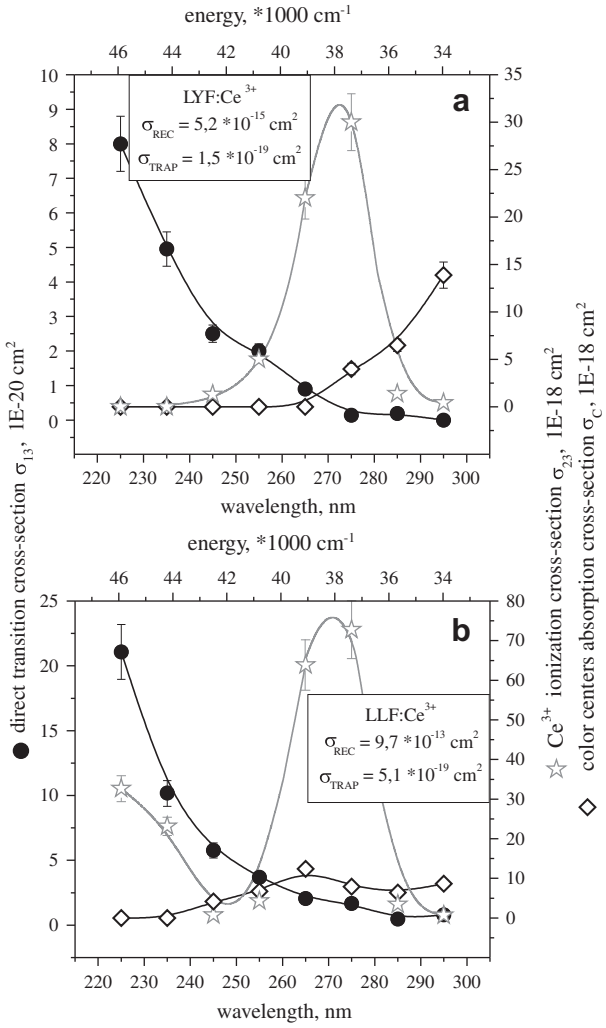

Fig. 3. Spectral distributions and values of one-photon (●) and two-photon (☆) Ce^{3+} excited-state ionization cross-sections, color centers ionization cross-section (◇), free charge carriers recombination (σ_{rec}) and trapping (σ_{trap}) cross-sections established as a result of numerical simulation of photoconductivity measurements. Symbols represent the simulation results, solid lines display the pattern.

(290–300 nm) corresponds to the weak photoconductivity signal. And on the contrary, between 255–280 nm, where Ce^{3+} ground-state absorption is negligible, ESP is nevertheless rather effective to result in large photoconductivity signal.

The spectral position of Ce^{3+} ESP band is determined by the relative positions of the energy levels of activator ions on the one hand and energy bands of the crystal lattice on the other. Thus, knowing that 4f–6s transition of Ce^{3+} in CaF_2 falls at ~143 nm [15], it is reasonable to assume that similarly positioned band in Ce^{3+}:$LiY_xLu_{1-x}F_4$ ($x = 0...1$) crystal series [16] corresponds to 4f–6s transitions of Ce^{3+} as well. Therefore, 270 nm ESP band derived here may be attributed to the transition between the lowest 5d and the higher-lying 6s level of Ce^{3+} ion, localized in the conduction band of the host (represented by the grey arrow on Fig. 4).

Besides, it was necessary to take into account the direct transition (one-photon ionization of Ce^{3+}) from the Ce^{3+} ground state to some level, localized just below or overlapping with the conduction band (transition represented by the black arrow on Fig. 4). We assume that this is one of the higher-lying 5d levels of Ce^{3+} ion. The probability of such direct transition, however, is two orders of magnitude lower than the probability of two-step process (see Fig. 3). The probability of recombination of the free electrons

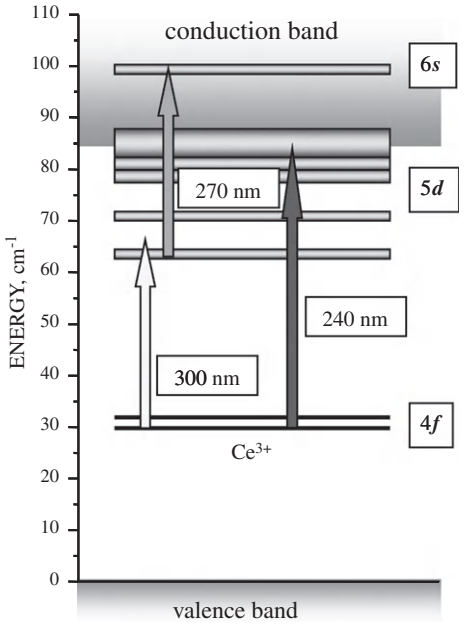

Fig. 4. Proposed energy level diagram for the joint system "Ce^{3+} ion–$LiYF_4$ crystal". White arrow represents the ground-state absorption of Ce^{3+}, light grey–two-photon stepwise ionization of Ce^{3+} due to excited-state absorption, dark grey –one-photon ionization of Ce^{3+}.

appeared to be two orders of magnitude higher for LLF compared to LYF, which explains the fact that LLF is much more stable in relation to the color centers formation.

Experimental and computing results allowed us to propose an energy level diagram of joint "Ce-ion – LYF crystal" system, presented on Fig. 4. The bandgap is assumed to be 10.5 eV (~84,700 cm^{-1}) wide in this crystal [17]. It is difficult to propose a similar diagram for LLF due to the lack of the reliable information on the width of its bandgap. Nevertheless, on the basis of the obtained results (higher Ce^{3+} ionization probability in LLF) and the assumption, that LLF has a wider bandgap than LYF [18], it is reasonable to assume, that the ground state of Ce^{3+} ions in LLF is localized higher than in LYF crystal. Previously proposed energy level diagram for Ce:LLF [19], however, does not seem likely to be correct, since it would not explain the 300 nm threshold of Ce^{3+} photoionization (it either should start under the excitation at much longer wavelengths in the IR region for the two-step process, or at much shorter ones for the one-step process).

5. Conclusions

Thus, photoconductivity measurements technique has been successfully applied to the investigation of photodynamic processes in $LiYF_4$:Ce^{3+} and $LiLuF_4$:Ce^{3+} (1 at.% in the melt) crystals in the 225–305 nm spectral region. Numerical values and spectral distributions of the important physical parameters characterizing these processes were determined as a result of fitting procedure. Energy level diagram of the "Ce^{3+} ion–$LiYF_4$ crystal" system has been proposed. The results are in agreement with the alternative investigations of these media by means of kinetic studies of Ce^{3+} luminescence and energy dependencies of Ce^{3+} absorption [20].

The value of photoconductivity measurements should not be underestimated. It would seem that pump-probe spectroscopy, which provides an excited-state absorption spectrum of the activator ions, exhausts all the issues in conducting similar research. Method of photoconductivity, however, accounts only for those doubly excited ions, which have been ionized and, therefore,

contributed in PDP. Thorough analysis of photoconductivity data on the basis of four-level model performed here is important not only to determine numerical values of physical parameters but to understand and correctly describe the general mechanisms involved in active medium undergoing intense UV excitation.

Acknowledgements

The authors are grateful for the Eiffel excellence scholarship granted by the French Ministry of Foreign and European Affairs. The research has been partially supported by the Federal Target Program "Research and scientific-pedagogical cadres of innovative Russia": Grants No. P989 and No. 02.740.11.0428. The authors are grateful to M. Marisov for the help in preparation of the samples.

References

[1] V.V. Semashko, M.A. Dubinskii, R.Yu. Abdulsabirov, S.L. Korableva, A.K. Naumov, A.S. Nizamutdinov, M.S. Zhuchkov, Proc. SPIE 4766 (17) (2001) 119–126.
[2] A.S. Nizamutdinov, V.V. Semashko, A.K. Naumov, R.Yu. Abdulsabirov, S.L. Korableva, M.A. Marisov, Phys. Solid State 47 (8) (2005) 1403–1405.
[3] C. Pedrini, F. Rogemond, D.S. McClure, J. Appl. Phys. 59 (4) (1986) 1196–1201.
[4] D.J. Ehrlich, P.F. Moulton, R.M. Osgood Jr., Opt. Lett. 4 (6) (1979) 184–186.
[5] M.A. Dubinskii, V.V. Semashko, A.K. Naumov, R.Yu. Abdulsabirov, S.L. Korableva, Laser. Phys. 4 (3) (1994) 480–484.
[6] M.F. Joubert, S.A. Kazanskii, Y. Guyot, J.C. Gacon, C. Pedrini, Phys. Rev. B 69 (2004) 165217.
[7] U. Happek, S.A. Basun, J. Choi, J.K. Krebs, M. Raukas, J. Alloys Compd. 303–304 (2000) 198–206.
[8] A.S. Nizamutdinov, V.V. Semashko, A.K. Naumov, S.L. Korableva, R.Yu Abdulsabirov, A.N. Polivin, M.A. Marisov, J. Lumin. 127 (2007) 71–75.
[9] A. Bensalah, M. Nikl, A. Vedda, K. Shimamura, T. Satonaga, H. Sato, T. Fukuda, G. Boulon, Radical Effect Def. Sol. 157 (2002) 563–567.
[10] A.S. Nizamutdinov, M.A. Marisov, V.V. Semashko, A.K. Naumov, R.Yu Abdulsabirov, S.L. Korableva, Phys. Solid State 47 (8) (2005) 1406–1408.
[11] V.V. Antonov-Romanovsky, Photoluminescence Kinetics of Crystals, Nauka, Moskow, 1966.
[12] A.S. Nizamutdinov, V.V. Semashko, A.K. Naumov, L.A. Nurtdinova, R.Yu Abdulsabirov, S.L. Korableva, V.N. Efimov, Phys. Solid State 50 (9) (2008) 1648–1651.
[13] K.S. Lim, D.S. Hamilton, J. Opt. Soc. Am. B 6 (7) (1989) 1401–1406.
[14] [14] B.D. Bunday, Basic Optimization Methods, Edward Arnold, London, 1984.
[15] E. Loh, Phys. Rev. 154 (2) (1967) 270–276.
[16] L.A. Nurtdinova, Ya Guyot, A.S. Nizamutdinov, V.V. Semashko, A.K. Naumov, S.L. Korableva, Uchenye zapiski Kazanskogo Gosudarstvennogo Universiteta, Estestvennye Nauki 150 (2) (2008) 185–190.
[17] J.C. Krupa, M. Queffelec, J. Alloys Compd. 250 (1997) 287.
[18] R. Moncorge, in: Ultraviolet Spectroscopy and UV Lasers, Marcel and Dekker, New York, 2002, pp. 337–395. .
[19] N.Yu Kirikova, M. Kirm, J.C. Krupa, V.N. Makhov, E. Negodin, J.Y. Gesland, J. Lumin. 110 (2004) 135–145.
[20] A.S. Nizamutdinov, V.V. Semashko, A.K. Naumov, S.L. Korableva, R.Yu Abdulsabirov, A.N. Polivin, M.A. Marisov, J. Lumin. 127 (2007) 71–75.